Hindawi
Shock and Vibration
Volume 2020, Article ID 9063929, 15 pages
https://doi.org/10.1155/2020/9063929

Research Article

Acoustic Emission Experimental Research of the Damage Characteristics of Raw Coal under Different Loading and Unloading Rates

Minbo Zhang,[1,2] Li Cui ,[2] Wenjun Hu,[2] Jinlei Du,[2] Zhen Zhang,[2] and Cuiling Wang[3]

[1]*Jizhong Energy Resources Co., Ltd., Xingtai 054000, China*
[2]*School of Xingfa Mineral Engineering, Wuhan Institute of Technology, Wuhan 430073, China*
[3]*Hubei Central China Technology Development of Electric Power Co., Ltd., Wuhan 430077, China*

Correspondence should be addressed to Li Cui; 1078413839@qq.com

Received 20 January 2020; Revised 6 June 2020; Accepted 8 July 2020; Published 23 July 2020

Academic Editor: Cristina Castejón

In this study, triaxial load failure experiments of coal samples under different strain rates and different confining pressure unloading rates were carried out using an RTX-1000 rock triaxial apparatus, and the acoustic emission characteristic parameters of a Micro-II acoustic emission imaging acquisition instrument were used to study the acoustic emission characteristics and damage deformation law of coals under different conditions. Damage models were constructed on the basis of the characteristic parameters to analyze the damage law of coal samples. Experimental results show that the acoustic emission (AE) counts and AE energy of the coal samples decrease, but the peak AE counts and peak AE energy increase with the increase in strain rates. The cumulative AE counts decrease from 9902 times to 6899 times, the peak counts increase from 209 times to 431 times, the cumulative AE energy decreases from 6986 aJ to 3786 aJ, and the peak AE energy increases from 129 aJ to 312 aJ. The overall level of the AE count rates and the AE energy of the coal samples decrease, but the peak AE counts and peak AE energy increase with the increase in unloading rates. The cumulative AE counts decrease from 18,689 times to 16,842 times, the peak AE count rates increase from 245 times/s to 535 times/s, the cumulative AE energy decreases from 9846 aJ to 7430 aJ, and the peak energy increases from 257 aJ to 587 aJ. The damage models are constructed on the basis of AE counts, and the comparative experimental and theoretical curves are analyzed to obtain a higher fitness close to 1. The damage threshold increases from 0.30 to 0.50 and from 0.34 to 0.55, and the damage amount increases from 0.50 to 0.60 and from 0.34 to 0.62 with the increase in strain rates and unloading rates. The research results have practical significance for revealing the mechanism of disaster occurrence in actual engineering excavation and proposing engineering measures to prevent coal rock damage and disaster occurrence.

1. Introduction

During coal mining, the coal body or rock mass is frequently influenced by different load rates caused by mining stress, tectonic stress, and construction disturbance because of the different conditions of coal seam occurrence and mining technical conditions. Different propulsion rates will have certain effects on the damage and acoustic characteristics of coal [1]. As China's shallow resources are becoming exhausted, more mines are beginning to excavate deep. The deformation and damage characteristics of surrounding rock gradually grow with the increase in mining depth, and the mechanical behavior and damage mechanism of coal-rock materials immensely vary [2]. The rock is in a state of three-way stress balance before excavation. After excavation, the rock side is unloaded, making it prone to rock burst, surrounding rock collapse, roof collapse, and other disasters. Different excavation methods, excavation speed, and excavation depth correspond to different mechanical and energy properties [3]. The onset and development of material damage are first detected by measuring acoustic emission (AE) counts [4] through damage experiments on material under loading. Many scholars at home and abroad have conducted numerous studies on this topic.

The rheological properties of polycrystalline salt rock were studied [5, 6] under different strain rate conditions. The results showed that the process of strain rate has great influence on the mechanical properties and crack propagation of polycrystalline salt rock. Liang et al. [7] tested the strain rate effect of the mechanical properties of salt rock and found that the safe and stable operation of a gas storage chamber can be ensured when the strain rate of the cavity wall is 10^{-5}–10^{-3} s^{-1}. Alam et al. [8] studied the mechanical behavior of sandstone under static and dynamic compressive strain rates. The peak stress, strain, and elastic modulus of sandstone increase with the increase in strain rate. Loading observations on fine sandstones and tuffs were performed [9, 10] at different strain rates. In-depth research was conducted [11–13] on the mechanical properties of rock under different loading strain rates. Vidya Sagar and Rao [14] selected four speed grades of 4, 5, and 6 MPa/s to conduct AE monitoring experiments on reinforced concrete beams during loading and studied the distribution characteristics of AE events at different loading rates. Zhang et al. [15] used numerical simulation to study the effect of strain rate on the number, size, and spatial distribution of AE events in prefractured rock-like materials. Wang et al. [16] used acoustic emission technology to study the damage evolution and fracture characteristics of dam concrete under different loading rates. Jiang et al. [17] explored the damage evolution and AE parameters of salt rock under different loading rates. Wang et al. [18] revealed the damage evolution law of impact-oriented sandstone under different strain rates.

Lau and Chandler [19] pointed out that the existing loading test path is inconsistent with the actual engineering, and using the unloading path is accurate to determine the rock mechanic parameters. Holcomb and Costin [20] applied the Kaiser effect principle to evaluate the surrounding rock stress state of rocks and used AE events to evaluate rock damage. Mansurov [21] predicted the type of rock failure on the basis on the AE phenomenon of rock mass destruction. Wu et al. [22] described the characteristics of excavation unloading damage and analyzed the applicability of Mohr–Coulomb yield criterion in the analysis of rock mass unloading damage. Tang and Ohtsu [23] used AE characteristic parameters and moment tensor methods to study the characteristics of tensile and shear failures during concrete failure. Chang and Lee [24] analyzed the damage variables of rock under triaxial loading conditions. Brzovic and Villaescusa [25] observed the process of underground engineering excavation for a long time period and found that the confining pressure slightly increases and then reduces. You and Hua [26] analyzed the three-axis unloading confining pressure. Gao et al. [27] studied the mechanical properties of marble loading and unloading. Wang et al. [28] conducted a triaxial experiment on the loading and unloading confining pressure of Beishan granite and investigated the failure mechanism of excavation disturbance on granite. Cong et al. [29] explored the AE characteristics of marble failure process under unloading confining pressure path. Qiu et al. [30] evaluated the effects of different unloading confining pressure rates on the macroscopic failure modes of marble samples. Zhang et al. [31] assessed the damage characteristics of gas-containing coal under different loading and unloading conditions.

The above studies lack the analysis of AE characteristics and damage of raw coal materials. In this study, the raw coal materials are subjected to different strain rates (0.005, 0.02, and 0.03%/min) and different unloading rates (0.1, 0.2, 0.4, and 0.6 MPa/s) through the AE experiments of triaxial load. The AE characteristic parameters during the experiments are analyzed, and the damage models are constructed to analyze the damage law of coal samples. This study has practical significance for revealing the damage and damage mechanism in coal mining and its application in engineering practice.

2. Experiment

2.1. Experimental Systems and Samples. An RTX-1000 high-temperature and high-pressure dynamic rock triaxial instrument with a maximum loading capacity of 1000 kN was used in the triaxial experiment (Figure 1). Strain sensors were attached to the rock triaxial apparatus, and six AE sensors (Figure 2) were mounted on the coal samples. The numbers in the figure represented the positions where the six AE sensors were installed. A Micro-II high-temperature and high-pressure AE imaging acquisition instrument was used for data acquisition. The AE device has six channels. The threshold value of this device is set to approximately 45 dB in accordance with the on-site noise condition. A pencil core is used to break the sound test and constantly adjust the threshold value, and the maximum setting is 70 dB. The mechanical and AE experiment systems collect data by connecting sensors, and the mechanical properties and AE characteristics of coal samples are related using the "external parameter." The "external parameter" collected by the AE experiment corresponds to the "axial stress" collected by the triaxial mechanical experiment. The coal mechanical and AE characteristic parameters are combined through this parameter for analysis.

The coal samples selected for this experiment (Figure 3) were taken from Jixi Mining, Chengshan Coal Mine. The mining area is approximately 8.2 km long from east to west and 3.5 km wide from north to south and covers an area of 37.8889 km^2. In accordance with the requirements of the regulations, the coal samples were processed into standard coal samples with a diameter of 50 mm and a height of 100 mm. The detailed parameters of the coal samples are shown in Table 1.

2.2. Experimental Plans and Principles. Two sets of experimental schemes were adopted to study the relationships between the stress and strain of coal samples under different strain rates and different confining pressure unloading rates.

(1) Option 1: the AE experiment of coal failure under different strain rates keeps the confining pressure constant at 15 MPa and applies the shaft to the strain rates of 0.005, 0.02, and 0.03%/min for coal samples

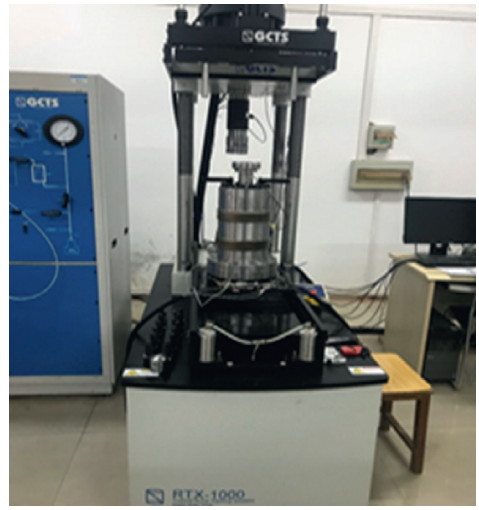

Figure 1: RTX-1000 high-temperature and high-pressure dynamic rock triaxial instrument.

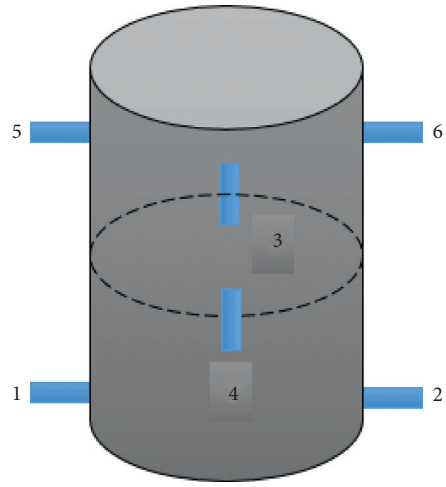

Figure 2: Layout of AE sensors.

1, 2, and 3, respectively. The coal samples are destroyed by pressing.

(2) Option 2: the AE experiment of coal failure under different confining pressure unloading rates maintains a confining pressure of 15 MPa and applies axial compression to 75% of the triaxial failure intensity of coal samples 4, 5, 6, and 7. In particular, the unloading of the confining pressure at 25 MPa to the raw coal failure is started at a rate of 0.1, 0.2, 0.4, and 0.6 MPa/s.

The strain sensors connected on the rock triaxial instrument and the AE sensors installed on the coal samples can transmit the deformation parameters of the coal samples to the computer in real time and obtain the characteristic parameters, such as stress, strain change, and AE of the coal samples during the experiment. In the unloading experiment, external stress is used to link the stress and strain of the coal samples with the AE characteristic parameters, and the relationships between the stress and strain of the coal samples and the AE characteristics under different unloading paths are analyzed to determine the deformation and failure characteristics of the coal samples.

After installing the coal samples on the rock triaxial instrument, the heat shrinkable tube and the coal samples should be tightly fitted with a hair dryer to prevent the silicone oil in the pressure chamber from leaking on the coal samples, thereby causing damage to the coal samples and the heat shrinkable tube. Six AE sensors are mounted on the surface, and the AE sensor is NANO30 with a peak frequency of 300 kHz.

3. Experimental Results

3.1. Effects of Strain Rates on the Strength and Deformation of Coal. The experimental results were analyzed, and the stress-strain curves were plotted, as shown in Figure 4. The stress and strain characteristics of coal samples under different strain rates during the experiment were analyzed.

In accordance with the experimental results, the peak intensities of coal samples 1, 2, and 3 are 23.31, 32.95, and 41.80 MPa, respectively. Two points are taken on the curved

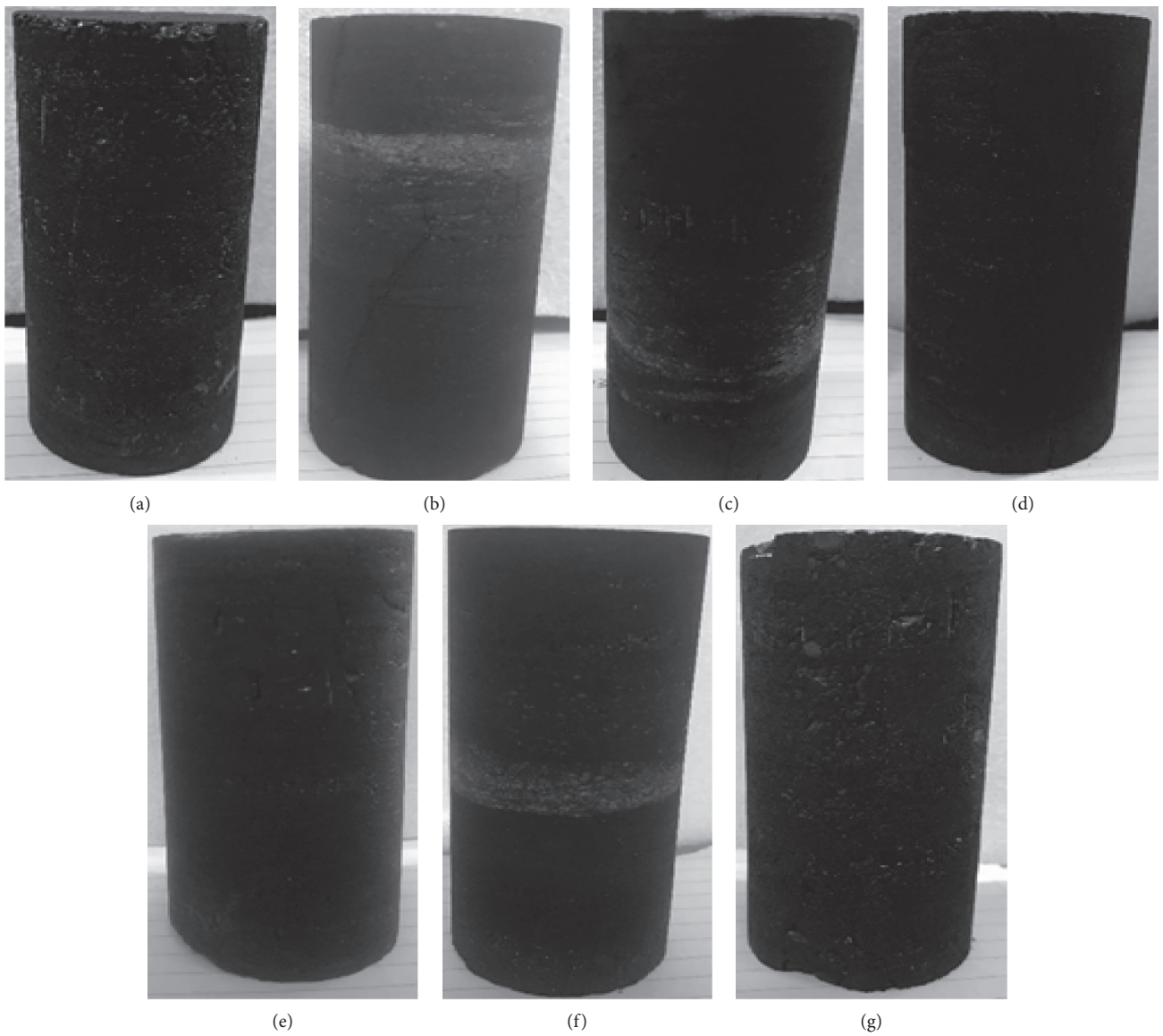

Figure 3: Coal samples. (a) No. 1 coal sample. (b) No. 2 coal sample. (c) No. 3 coal sample. (d) No. 4 coal sample. (e) No. 5 coal sample. (f) No. 6 coal sample. (g) No. 7 coal sample.

Table 1: Parameters of coal samples.

Number of experiment groups	Number	Strain rate (%/min)	Diameter (mm)	Height (mm)	Cell pressure (MPa)	Axial pressure (MPa)
First group	1	0.005	50.33	101.50	15	Load to destruction
	2	0.02	50.57	101.37		
	3	0.03	50.43	101.35		
Number of experiment groups	Number	Confining pressure unloading rate (MPa/s)	Diameter (mm)	Height (mm)	Cell pressure (MPa)	Axial pressure (MPa)
Second group	4	0.1	50.53	101.30	15	25
	5	0.2	50.33	101.35		
	6	0.4	50.47	101.37		
	7	0.6	50.53	101.43		

straight line segment shown in Figure 4. The elastic moduli of coal samples 1, 2, and 3 calculated by the program are 3.23, 5.70, and 6.19 GPa, respectively. Poisson's ratios of coal samples 1, 2, and 3 are 0.34, 0.31, and 0.25, respectively. The ultimate strain values of coal samples 1, 2, and 3 are 0.26, 0.38, and 0.40, respectively. From the data analysis, the peak intensities and elastic modulus of the coal samples increase with the increase in strain rates, and Poisson's ratios

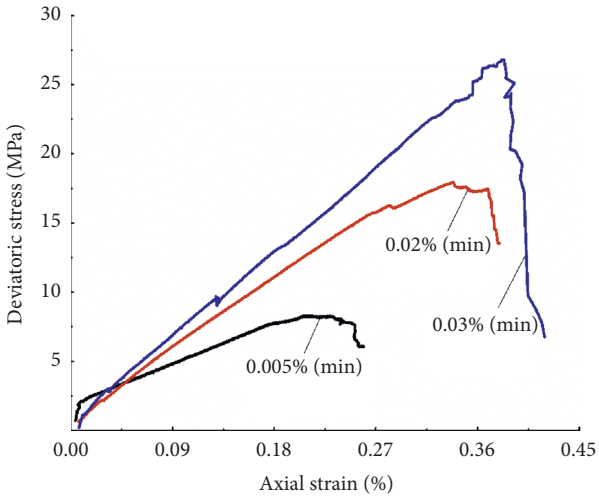

Figure 4: Stress and strain process curves.

decrease with the increase in elastic modulus when the confining pressure is constant. This condition is because the small cracks inside the coal samples are fully developed and expanded when the strain rates are low. Thus, the internal damage of the coal samples before the peak intensity is reached, resulting in a decrease in compressive intensity and a high strain rate. Under this condition, the microcracks inside the coal samples cannot be fully developed and expanded, thereby improving the integrities and bearing capacity of the coal samples. The ultimate strain values of coal samples increase with the increase in strain rates, indicating that the fracture deformation degree of coal samples increases accordingly. From the macroscopic point of view, the cracks of the coal samples are deepened, and the fragments are increased, as shown in Figure 5.

3.2. Effects of Strain Rates on AE Characteristic Parameters. Different strain rates have an effect on AE characteristic parameters during the coal sample AE experiment. In this process, the damage inside the coal samples can be expressed by AE counts and AE energy, as shown in Figures 6 and 7.

As shown in Figures 6 and 7, the AE counts and the AE energy during the experiments of coal samples 1, 2, and 3 show the same trend. In particular, in the elastic compaction stage, only few AE events are generated, accompanied by a small amount of AE counts and AE energy generation, and the internal damage of the coal samples is small because the cracks inside the coal sample are compacted and closed. The deformation of coal samples enters the elastic deformation stage, and the closure of the original cracks in the coal samples increases their integrity. At this time, the AE counts and AE energy remain small, showing only a slight growth trend. The internal damage of the coal samples is relatively small. The coal samples enter the plastic deformation stage, and a large number of new cracks appear inside the coal samples as the loading progresses. These cracks begin to stabilize and gradually expand, and the AE counts and AE energy begin to grow steadily. Before the coal samples reach the peak intensity, macroscopic cracks began to occur, and the AE counts and AE energy sharply increase, reaching the maximum at the peak intensity of the coal samples. At this time, the cracks inside the coal samples gradually developed to instability failure.

Under the same conditions, the strain rates are different, and the effects on AE counts and AE energy generation of coal samples are also different. The effects are summarized as follows:

(1) At different strain rates, the peak AE counts and the peak AE energy during the rupture of coal samples increase with increasing strain rates. The peak AE count is 209 times, and the peak AE energy is 129 aJ when the strain rate is 0.005%/min. The peak AE count is 342 times, and the peak AE energy is 205 aJ when the strain rate is 0.02%/min. The peak AE count is 431 times, and the peak AE energy is 312 aJ when the strain rate is 0.03%/min. The increase in peak AE counts and peak AE energy is because the rates of the development of cracks in the coal samples increase, and the impacts of coal sample damage increase with the increase in strain rates, thereby accelerating the damage of coal.

(2) Under different strain rates, the cumulative AE counts and the cumulative AE energy during the failure of coal samples decrease with increasing strain rates. The cumulative AE counts are 9902 times, and the cumulative AE energy is 6986 aJ when the strain rate is 0.005%/min. The cumulative AE counts are 8431 times, and the cumulative AE energy is 4472 aJ when the strain rate is 0.02%/min. The cumulative AE counts are 6899 times, and the cumulative AE energy is 3786 aJ and when the strain rate is 0.03%/min. The decrease in the cumulative AE counts and cumulative AE energy is because the cracks inside the coal samples are not fully developed and expanded, the AE activities are reduced, and the internal accumulated energy is not fully released with the increase in strain rates.

3.3. Analysis of the Effects of Different Confining Pressure Unloading Rates. Axial pressure was applied to 75% of the peak stress, that is, 25 MPa, and the confining pressure of 15 MPa was unloaded at different unloading rates to obtain the experimental results of coal sample Nos. 4, 5, 6, and 7. The peak stress of coal samples under different confining pressure unloading rates is slightly different. The peaks of AE counts and AE energy increase, the AE count rates increase from 245 times/s of 0.1 MPa/s to 535 times/s at 0.6 MPa/s, and the AE energy increases from 257 aJ to 587 aJ with the increase in unloading rate. The peak times of AE characteristic parameter decrease with the increase in the unloading rate from 1132.90 s to 1007.81 s. This finding shows that the difference in unloading rates does not change the bearing capacity of the coal samples but changes the time of coal sample damage and affects the AE characteristics, as shown in Figures 8 and 9.

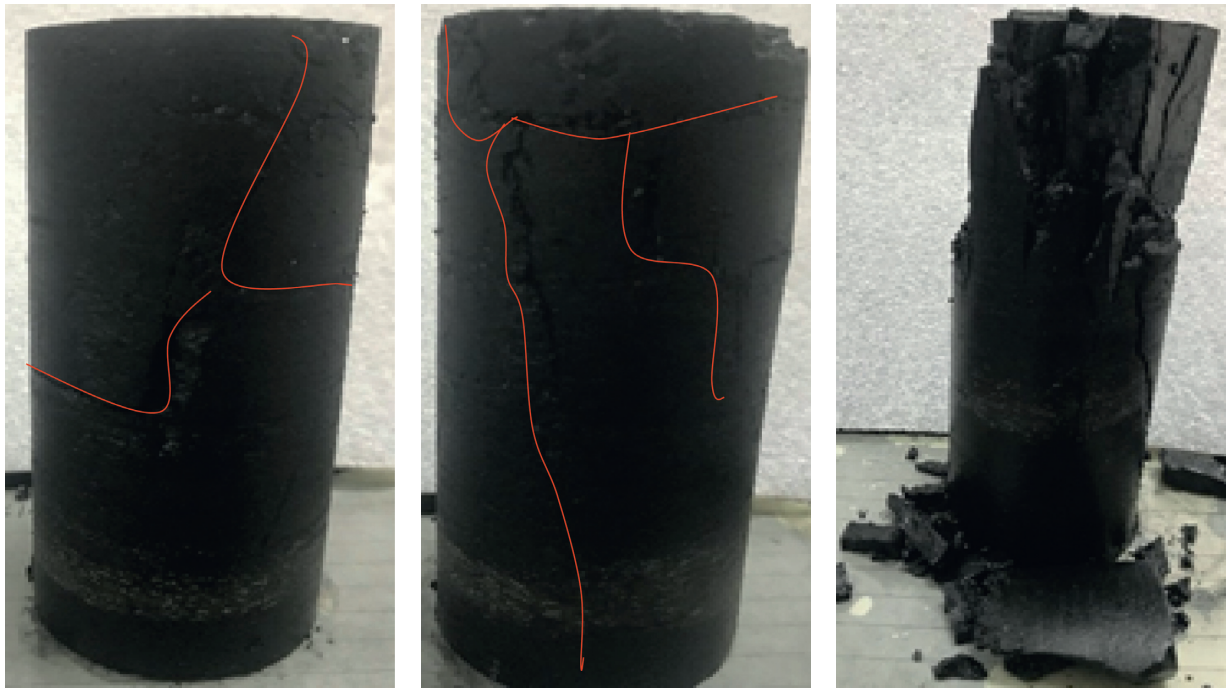

(a) (b) (c)

Figure 5: Destruction states of coal samples with different strain rates. (a) No. 1 coal sample. (b) No. 2 coal sample. (c) No. 3 coal sample.

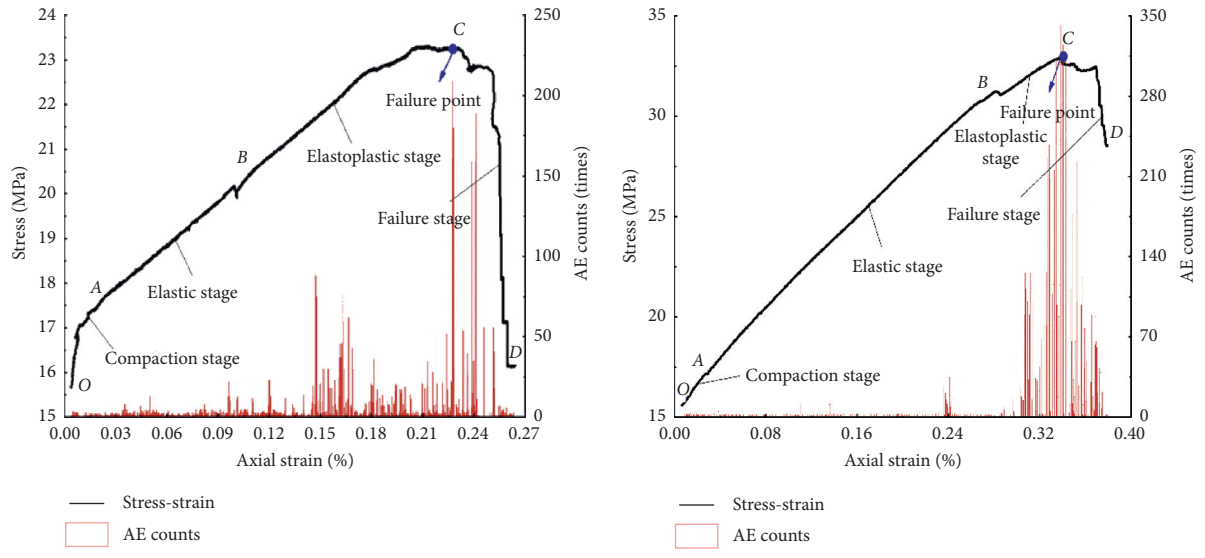

Figure 6: Continued.

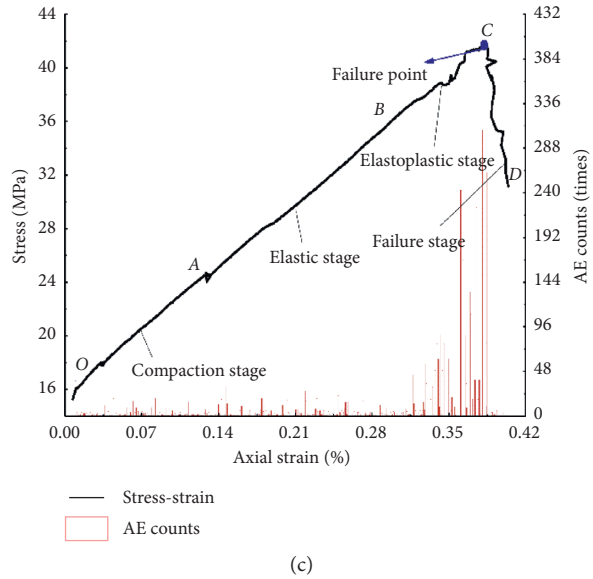

(c)

Figure 6: Corresponding curves of AE counts under different strain rates. (a) 0.005%/min strain rate. (b) 0.02%/min strain rate. (c) 0.03%/min strain rate.

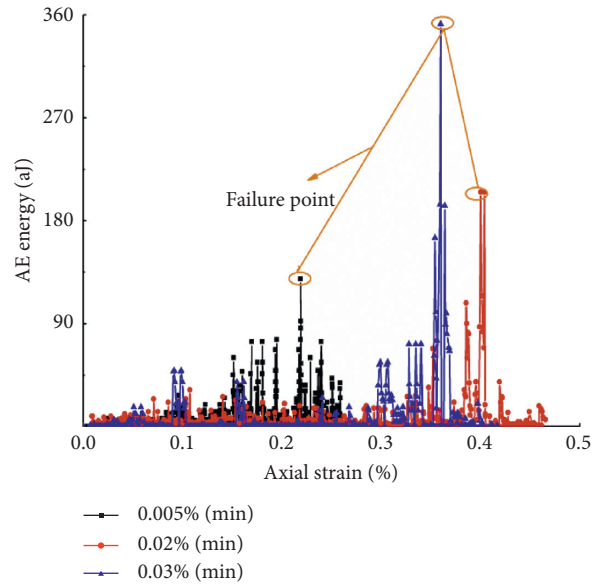

Figure 7: Corresponding curves of AE energy strain under different strain rates.

Comparing the stress-time-AE count rates curves of Figure 8 and the AE energy curves of the four coal samples in Figure 9, we have the following.

In the initial elastic compaction stage, the AE count rates and AE energy of the coal samples are relatively small. The AE count rates and the AE energy steadily increase but are still at a low level after entering the elastic stage, and the growth rates of the curves at this time are relatively stable. The increases in AE count rates and AE energy are evident when approaching the unloading point, and the growth rates of the curves increase at this time. At the unloading point, the AE count rates and AE energy have a decreasing trend. After the unloading is started, the AE count rates and AE energy sharply increase, and the growth rates of the curves are higher than those at each stage. The peaks of the AE count rates and AE energy appear when the coal samples are destroyed, the maximum value occurs, and the coal samples are destroyed.

After the unloading point, different unloading rates have different effects on the AE characteristics of the coal samples:

(1) The time from the unloading point to the failure point is approximately 120 s, and the stress difference is increased by approximately 14 MPa when the

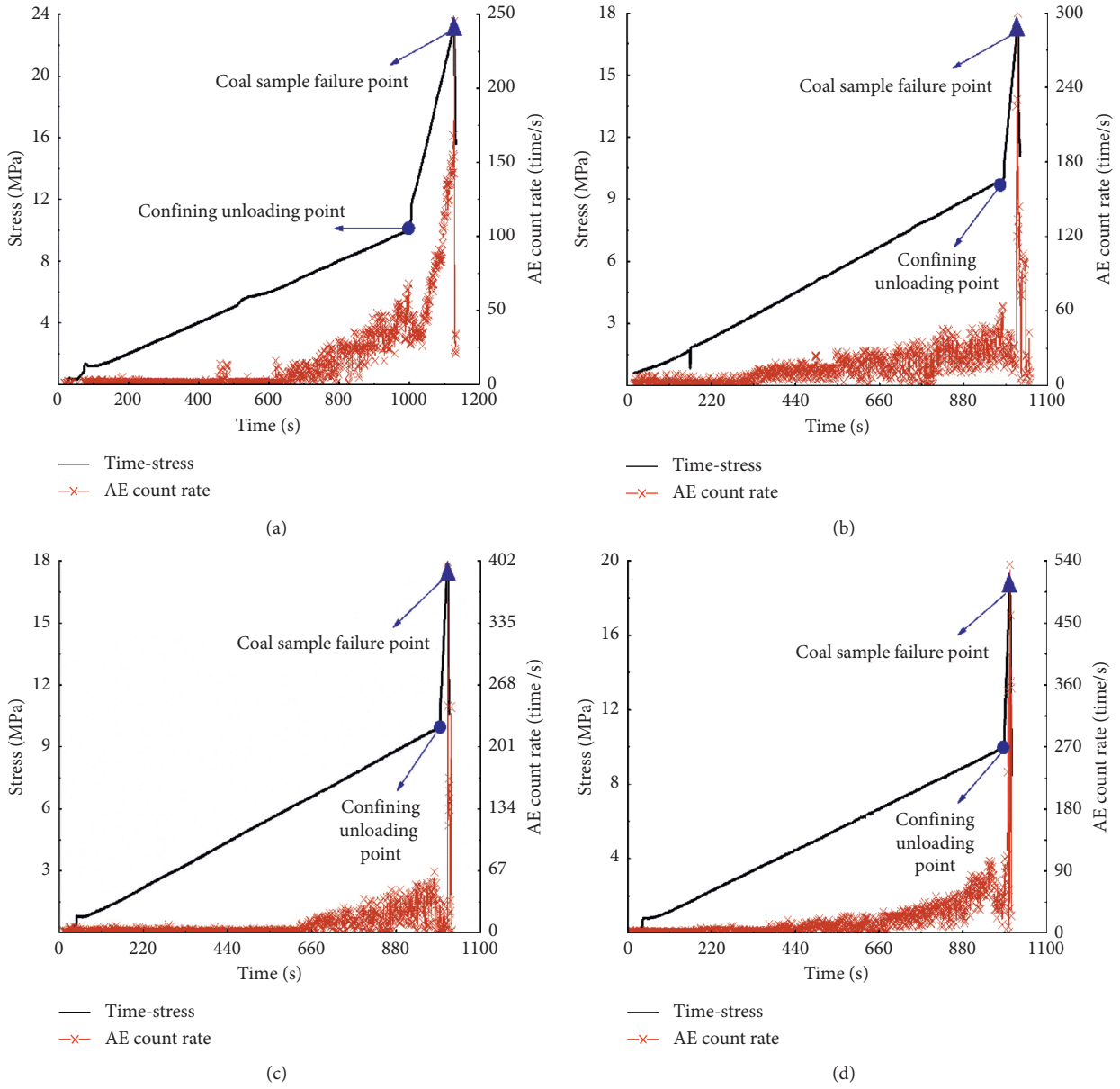

Figure 8: Corresponding curves of AE count time under different unloading rates. (a) 0.1 MPa/s unloading rate. (b) 0.2 MPa/s unloading rate. (c) 0.4 MPa/s unloading rate. (d) 0.6 MPa/s unloading rate.

unloading rate is 0.1 MPa/s. The coal sample is unloaded when the unloading rate is 0.2 MPa/s. The duration from the charge point to the failure point is approximately 100 s, and the stress difference is increased by approximately 7 MPa. The time from the unloading point to the failure point of the coal sample is approximately 50 s, and the stress difference is increased by approximately 8 MPa when the unloading rate is 0.4 MPa/s. The time from the unloading point to the failure point of the coal sample is approximately 30 s, and the stress difference is increased by approximately 9 MPa when the unloading rate is 0.6 MPa/s. This finding shows that the greater the unloading rate is, the faster the confining pressure decreases, the shorter the coal sample destruction needs to last, and the more severe the coal sample damage will be. The change in unloading rate does not change the bearing capacity of the coal sample. The coal sample is destroyed when the stress difference increases by approximately 10 MPa, and the state of the coal sample after the destruction of Figure 10 is combined. From the macroscopic point of view, the fragments of the coal samples are increased, as shown in Figure 10.

(2) The AE count rate gradually increases from the beginning of 1 time/s and increases to 47 times/s from 994 s, and the AE count rate decreases to 35 times/s when the unloading rate is 0.1 MPa/s. The AE count rate rapidly increases and reaches the peak of 245 times/s when the unloading point is reached, and

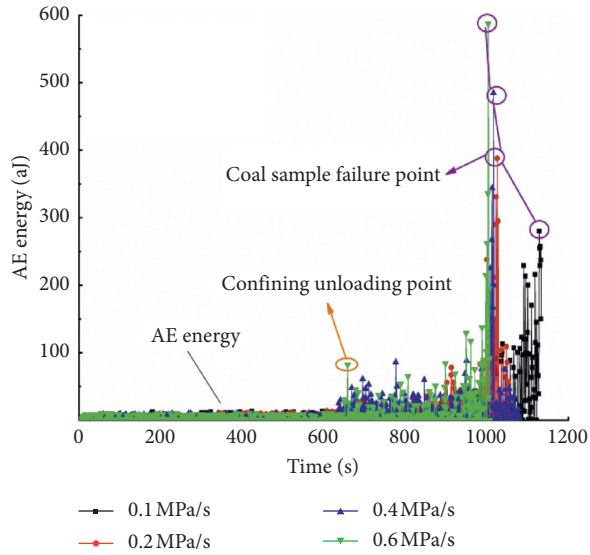

Figure 9: Corresponding curves of AE energy time under different unloading rates.

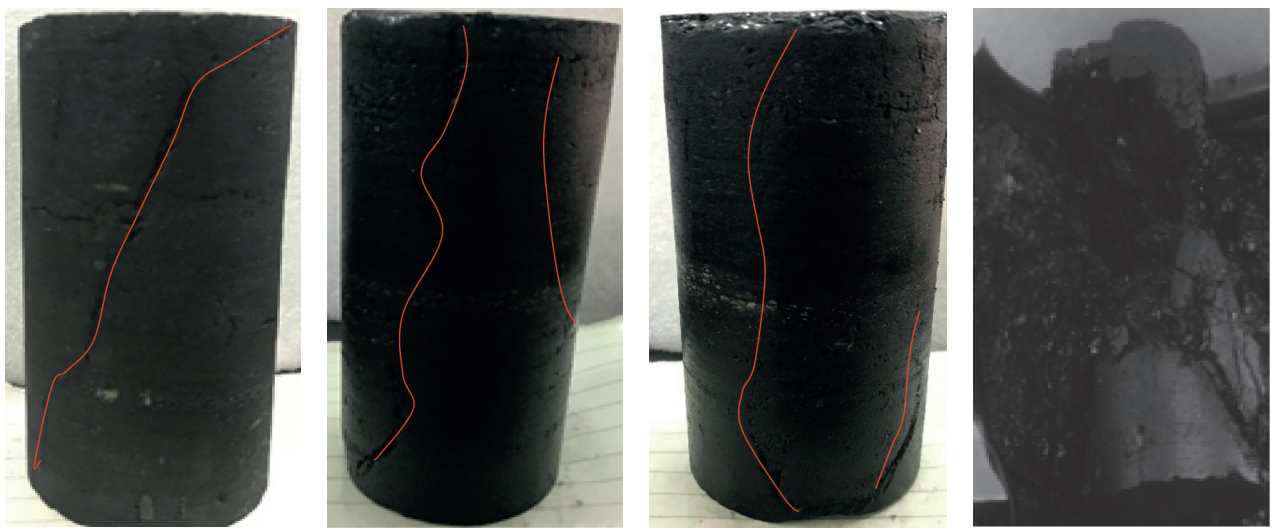

Figure 10: Destruction status of coal samples at different unloading rates. (a) No. 4 coal sample. (b) No. 5 coal sample. (c) No. 6 coal sample. (d) No. 7 coal sample.

the duration is approximately 35 s. The cumulative count is 18,689 times, the peak AE energy is 257 aJ, and the cumulative AE energy is 9846 aJ. The AE count rate gradually increases from the beginning of 2 times/s and increases to approximately 40 times/s from 984 s when the unloading rate is 0.2 MPa/s, and the AE count rate decreases to 23 times/s when the unloading point is reached. The AE count rate rapidly increases and reaches the peak value of 300 times/s, and the duration is approximately 25 s. The cumulative count is 17,331 times, the peak AE energy is 388 aJ, and the cumulative AE energy is 9617 aJ. The AE count rate gradually increases from the beginning of 1 time/s and increases to approximately 36 times/s from 993 s when the unloading rate is 0.4 MPa/s, and the AE count rate decreases to 19 times/s when the unloading point is reached. The AE count rate rapidly increases and reaches the peak value of 401 times/s, and the duration is approximately 24 s. The cumulative AE count is 17,224 times, the peak AE energy is 485 aJ, and the cumulative AE energy is 8561 aJ. The AE count rate from the beginning of 1 time/s gradually increases to 43 times/s at around 988 s when the unloading rate is 0.6 MPa/s, and the AE count rate decreases to 30 times/s when the unloading point is reached. The AE count rate rapidly increases and reaches the peak value of 535 times/s, and the duration is approximately 20 s. The cumulative count is 16,842 times, the peak AE energy is

587 aJ, and the accumulated AE energy is 7430 aJ. The analysis shows that the other conditions are the same, where the larger the confining pressure unloading rates of the coal samples are, the lower the AE count rates and the overall level of the AE energy are. This condition is because the larger the unloading rates are, the faster the confining pressure decreases, resulting in the interior damage of the coal samples. The cracks are not fully developed and expanded, and the AE intensity is low. Thus, the AE count rates and AE energy are low. The peak AE count rates and the peak AE energy of the coal samples increase because the increase in unloading rates leads to the increase in the impacts of the coal sample damage, thereby accelerating the damage process and raw coal damage.

Although the cumulative AE counts and cumulative AE energy decrease with the increase in strain rates, the average energy of a single impact increases. Similarly, the cumulative AE counts and cumulative AE energy decrease, whereas the average energy of a single impact increases with the increase in confining pressure unloading rates. This condition indicates that the larger the strain rates are, the larger the confining pressure unloading rates are, the greater the average energy released during the development of cracks is, and the greater the impact damage to the coal samples is. Therefore, the excavation speed in engineering practice can be controlled to avoid the occurrence of disasters, such as impact. For example, in coal mining, the energy released by the coal during destruction and the possibility of occurrence of a rock explosion are large when the excavation speed is extremely fast.

4. Analysis of Coal Damage Based on AE

4.1. Establishment of Damage Model. Kachanov defined [32] the damage variable as

$$D = \frac{A_d}{A}, \tag{1}$$

where A_d is the area of the microdefect on the load-bearing section and A is the area of the fracture without initial damage.

When the cumulative AE of the entire section A of the nondestructive material is C_0, the AE ringing count C_w at the time of destruction per unit area of the microelement is

$$C_w = \frac{C_0}{A}. \tag{2}$$

When the section damage area reaches A_d, the cumulative AE ringing count C_d is

$$C_d = C_w A_d = \frac{C_0}{A} A_d. \tag{3}$$

Thus, we have

$$D = \frac{C_d}{C_0}. \tag{4}$$

The damage variable is modified as

$$D = D_U \frac{C_d}{C_0}, \tag{5}$$

where D_U is the damage threshold. In the formula, the value of C_0 is the cumulative AE ringing count when the damage variable reaches D_U. For the simplicity of calculation, the damage threshold is expressed as

$$D_U = 1 - \frac{\sigma_C}{\sigma_P}, \tag{6}$$

where σ_P is the peak intensity and σ_C is the residual intensity. In accordance with formula (6), the damage thresholds of coal sample Nos. 1, 2, and 3 are 0.30, 0.39, and 0.50, respectively. The damage thresholds of coal sample Nos. 4, 5, 6, and 7 are 0.34, 0.35, 0.39, and 0.55, respectively.

In accordance with formulas (5) and (6), the damage strain curves of coal samples are obtained, and the theoretical curves of damage strain are selected using an exponential function. The exponential function is selected for fitting because it accords with the growth law of coal damage strain experiment curve. The law of growth is that the curve begins to grow slowly and the curve grows rapidly.

The equation for the theoretical curve of coal strain damage with different strain rates is

$$D = D_0 + Ae^{-\sigma/b}. \tag{7}$$

The equation for the theoretical curve of coal sample damage at different confining pressure unloading rates is

$$D = D_0 + Ae^{-t/b}. \tag{8}$$

The specific parameters in the theoretical curve are shown in Table 2.

D_0 is the original damage of the coal samples, A and b are constant quantities, σ is the axial strain, %, and t is the time, s.

4.2. Analysis of Damage Evolution. In accordance with the theoretical equation of damage, the damage curve was fitted, and the experimental and theoretical curves were compared and analyzed, as shown in Figures 11 and 12.

Figure 11 shows the comparison of theoretical and experimental curves of coal sample damage under different strain rates. The damage strain curves can be divided into three stages on the basis of AE counts. In the initial stage, the coal samples are compacted and closed, no new cracks are found in the coal samples, and the AE activity and AE counts are few. At this time, the coal sample damage is small. The coal sample damage enters a stable development stage, and the new cracks generated inside the coal samples begin to expand and develop. The generated AE counts grow steadily, and the internal damage of the coal samples increases when they deform in the elastic and plastic deformation stages. The coal samples enter the accelerated development stage, the crack inside the coal sample rapidly develops, converges, and penetrates, the AE counts sharply increase, the coal sample damage exponentially increases, and the coal samples show macroscopic damage with continuous loading. The entire curve roughly exhibits a linear-exponential increase.

Table 2: Specific parameters of the theoretical curve.

	D_0	A	b	Fit
0.005% (min)	−0.050	0.048	−0.106	0.99
0.02% (min)	0.019	0.013	−0.100	0.97
0.03% (min)	0.014	1.63×10^{-4}	−0.048	0.97
0.1 MPa/s	0.002	3.89×10^{-4}	−168.08	0.99
0.2 MPa/s	−0.042	0.032	−405.31	0.99
0.4 MPa/s	−0.008	0.009	−275.89	0.99
0.6 MPa/s	0.002	0.004	−198.90	0.99

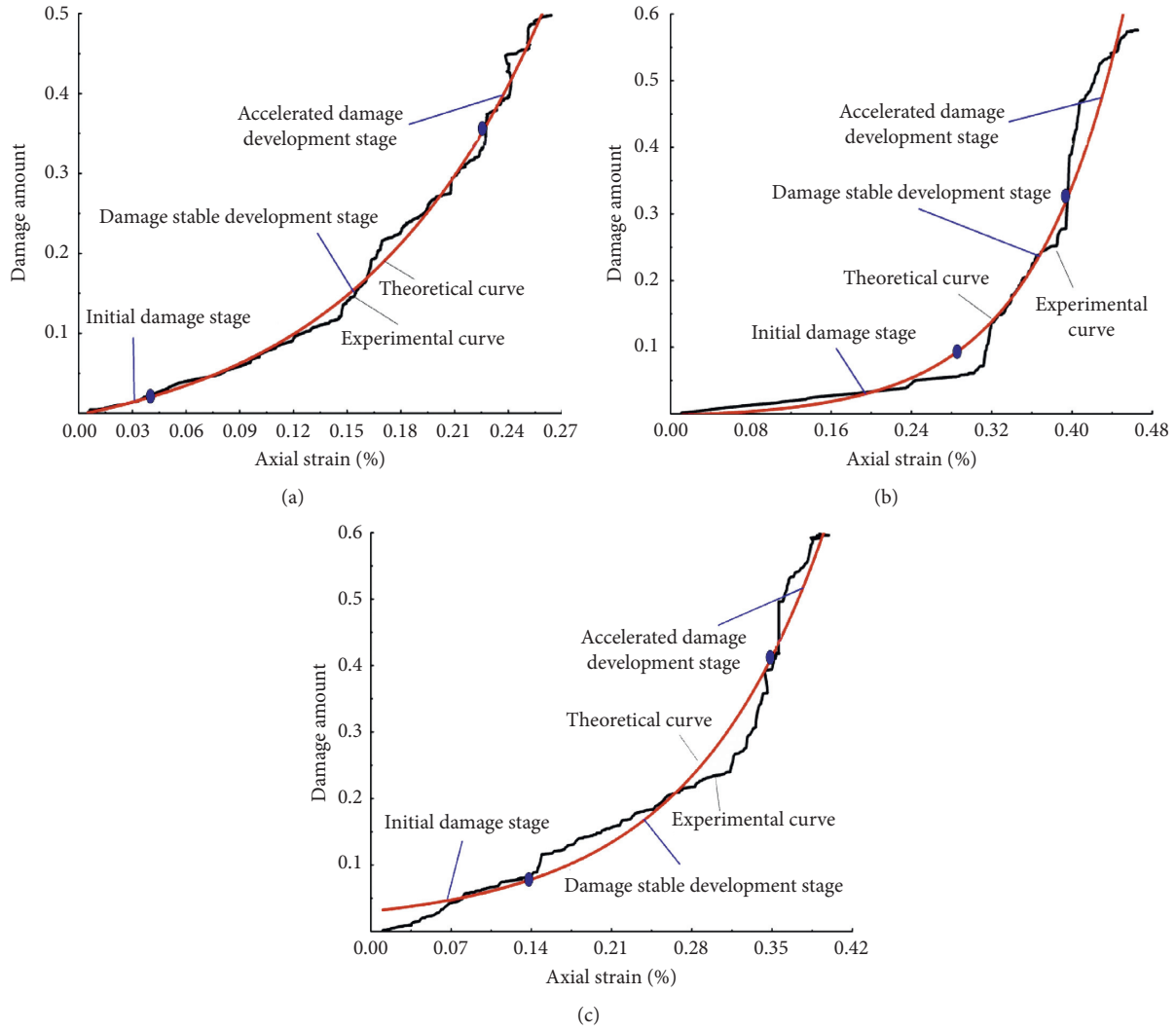

Figure 11: Comparison of theoretical and experimental curves of coal sample damage under different strain rates. (a) 0.005%/min strain rate. (b) 0.02%/min strain rate. (c) 0.03%/min strain rate.

The maximum damage amount is 0.50 when the strain rate is 0.005%/min, the maximum damage amount is 0.57 when the strain rate is 0.02%/min, and the maximum damage amount is 0.60 when the strain rate is 0.03%/min. This finding shows that the damage of coal samples increases with the increase in strain rates. This condition is because the larger the strain rates, the faster the axial stress loading, the higher the energy released by the coal samples during damage, and the more serious the damage of the coal samples. The corresponding damage amount is large.

Figure 12 shows the comparison of theoretical and experimental curves of coal sample damage under different unloading rates. Similarly, the damage curves can be roughly divided into two stages on the basis of AE counts. Before the unloading point, the AE activity inside the coal samples and the AE counts are few, and the damage inside the coal

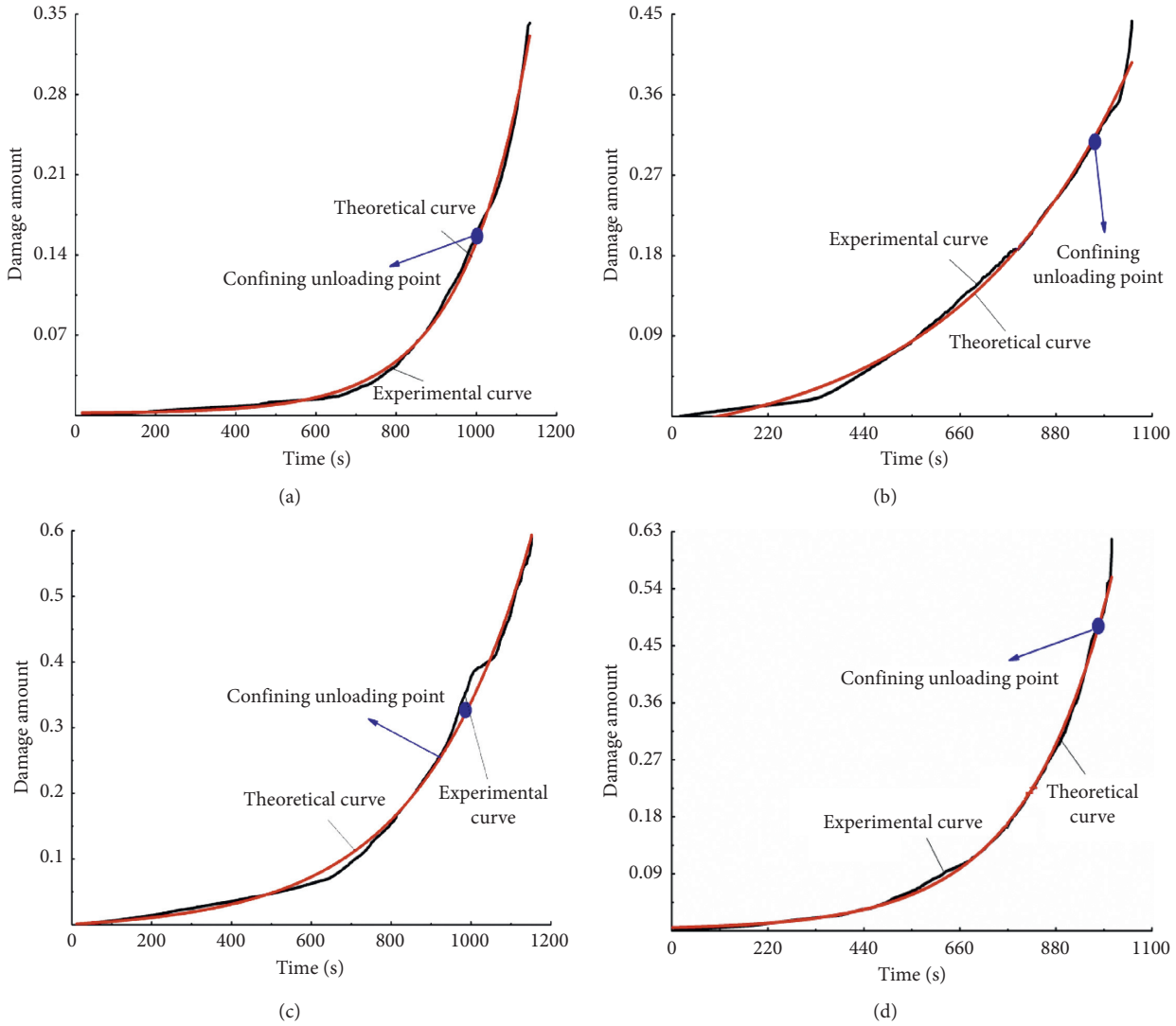

FIGURE 12: Comparison of theoretical and experimental curves of coal sample damage under different unloading rates. (a) 0.1 MPa/s unloading rate. (b) 0.2 MPa/s unloading rate. (c) 0.4 MPa/s unloading rate. (d) 0.6 MPa/s unloading rate.

samples is small. The AE activity sharply increases, and the generated AE counts rapidly increase when the coal samples start unloading. The internal damage of the coal samples exponentially increases, and the coal samples undergo macroscopic damage. The entire curve roughly exhibits a linear-exponential increase.

The maximum damage is 0.34, 0.44, 0.59, and 0.62 when the unloading rates are 0.1, 0.2, 0.4, and 0.6 MPa/s, respectively. The damage amount of the coal samples increases with the increase in confining pressure unloading rates. This condition is because the greater the unloading rates are, the faster the internal crack growth rates of the coal samples are and the faster the confining pressure decreases, resulting in a rapid increase in the AE rates when the coal samples are destroyed, releasing more energy, and the more serious the coal sample damage, the larger the corresponding damage amount.

In accordance with the fitting degree of each coal sample in Table 2, the coal rock damage failure model based on AE count better simulates the regularity characteristics of coal rock damage and deformation, the fitting degree is high, and the fits of seven coal samples are all close to one. In [33], the critical value of rock damage is $0.2 \leq D_U \leq 0.8$, and the experiment results show that the damage critical value of seven coal samples is within the range. The damage critical value and damage amount of coal samples increase with the increase in strain and unloading rates.

The local variation of coal rock is not considered because the damage of coal sample is discontinuous during the experiment and the theoretical curve is a function of continuous change. Therefore, the theoretical curve has certain deficiencies in describing coal sample damage and deformation. The damage model established on the basis of AE

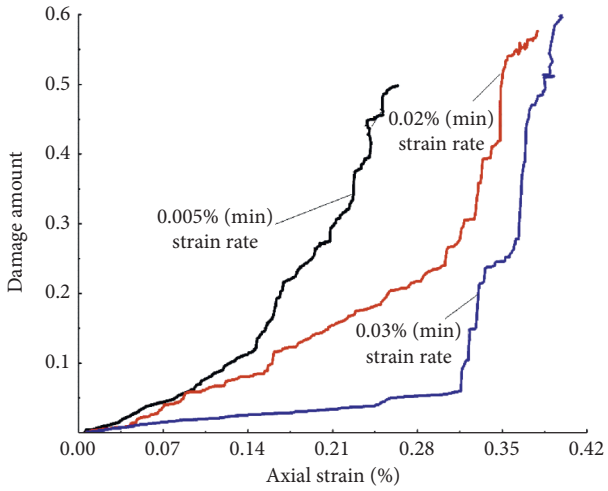

Figure 13: Corresponding curves of damage strain under different strain rates.

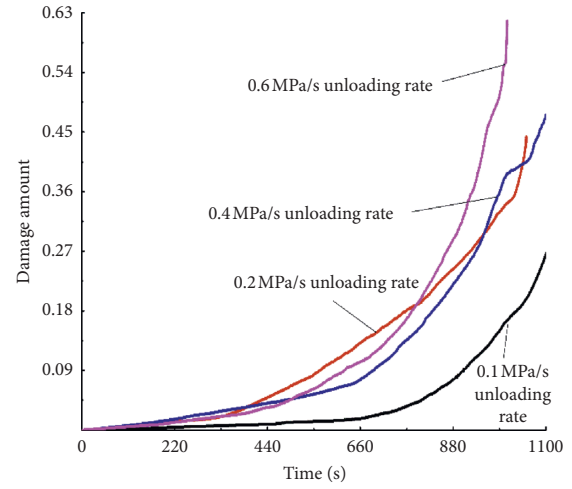

Figure 14: Corresponding curves of damage time under different unloading rates.

count has certain errors and needs to be continuously improved in subsequent research.

5. Discussion

The damage-strain relationship curves of coal samples under different strain rates are compared (Figure 13). The axial strain when the coal sample is broken is 0.26, and the damage amount is 0.50 when the strain rate is 0.005%/min. The axial strain when the coal sample is broken is 0.38, and the damage amount is 0.57 when the strain rate is 0.02%/min. The axial strain when the coal sample is broken is 0.40, and the damage is 0.60 when the strain rate is 0.03%/min. The analysis shows that the strain value of the coal samples at the time of failure appears to increase, and the amount of damage increases with the increase in strain rates. This condition is because the microcracks inside the coal samples are fully developed, and the expansion causes large damage in the coal samples at low strain rates. At high strain rates, the cracks in the coal samples cannot be fully developed and expanded, thereby improving the integrity and bearing capacity of the coal samples. With the increase in strain rates, the degree of crushing and deformation of the coal samples increases, the cracks of the coal samples are deepened, and the number of fragments increases.

The damage time relationship curves of coal samples under different confining pressure unloading rates are compared (Figure 14). The time when the coal sample is broken is 1132.90 s, and the damage amount is 0.34 when the unloading rate is 0.1 MPa/s. The time when the coal sample is broken is 1053.26 s, and the damage is 0.44 when the unloading rate is 0.2 MPa/s. The time when the coal sample is broken is 1151.88 s, and the damage is 0.59 when the unloading rate is 0.4 MPa/s. The time when the coal sample is broken is 1007.81 s, and the damage amount is 0.62 when the unloading rate is 0.6 MPa/s. The analysis shows that the time required for coal samples to fail appears to decrease with the increase in the unloading rates. This condition is because the larger the unloading rates, the shorter the time for cracks to develop, thereby allowing the cracks to form rapidly and reach failure.

6. Conclusions

In this study, AE experiments of coal samples under different strain rates and different confining pressure unloading rates were conducted to study the mechanical and AE characteristic parameters, and the deformation damage of coal samples was analyzed. The conclusions are summarized as follows:

(1) The peak intensity and elastic modulus of the coal samples increase with the increase in strain rates, and Poisson's ratios of the coal samples decrease with the increase in elastic modulus.

(2) The cumulative AE counts and cumulative AE energy of the coal samples decrease, but the peak AE counts and peak AE energy increase with the increase in strain rates.

(3) Different confining pressure unloading rates have no effect on the bearing capacity of coal samples but have a significant impact on the AE characteristic parameters of coal samples. The cumulative AE count rates and cumulative AE energy of the coal samples decrease, and the peak AE count rates and the peak AE energy increase with the increase in unloading rates.

(4) The coal sample damage model is established on the basis of AE count, and the damage deformation law of the coal samples is better simulated. The greater the strain rates, the greater the damage of the coal samples; the greater the unloading rates, the greater the damage of the coal samples.

Data Availability

The data used to support the findings of this study have not been made available because the original data relate to the

intellectual property rights of the author, and all the original data cannot appear in the paper, and the experimental data that cannot appear is related to privacy.

Conflicts of Interest

All authors declare no conflicts of interest.

Acknowledgments

This work was supported by the Hebei Postdoctoral Innovation Project (no. B2019005005), Science and Technology Research Program Young Talents Project of the Hubei Provincial Department of Education (no. Q20171508), Wuhan Institute of Technology Science Fund (no. K201855), and Wuhan Institute of Technology Graduate Education Innovation Fund (no. CX2019098).

References

[1] Z. Zhao, K. Zhao, and X. Wang, "Study on mechanical properties and damage evolution of coal-like rock under different loading rates," *Coal Science and Technology*, vol. 45, no. 10, 2017.

[2] J. Xu, R. Zhou, D. Song et al., "Deformation and damage dynamic characteristics of coal–rock materials in deep coal mines," *International Journal of Damage Mechanics*, vol. 28, no. 1, pp. 58–78, 2017.

[3] G. Liu, J. Zhao, and H. Song, "Analysis of roadway stability in jointed rock mass," *Journal of Central South University: Science and Technology*, vol. 44, no. 7, pp. 2910–2918, 2013.

[4] S. Murakami, K. Hayakawa, and Y. Liu, "Damage evolution and damage surface of elastic-plastic-damage materials under multiaxial loading," *International Journal of Damage Mechanics*, vol. 7, no. 2, pp. 103–128, 1998.

[5] S. T. Horseman and J. Handin, "Triaxial-compression tests on rocksalt at temperatures from 50° to 200°C and strain rates from 10^{-4} to 10^{-9}/s," *The Brittle-Ductile Transition in Rocks*, Wiley, Hoboken, NJ, USA, pp. 103–110, 1990.

[6] R. C. M. W. Franssen, "The rheology of synthetic rocksalt in uniaxial compression," *Tectonophysics*, vol. 233, no. 1-2, pp. 0–40, 1994.

[7] W. G. Liang, Y. S. Zhao, and S. G. Xu, "Effect of strain rate on the mechanical properties of salt rock," *International Journal of Rock Mechanics and Mining Sciences*, vol. 48, no. 1, pp. 161–167, 2011.

[8] M. S. Alam, T. Chakraborty, V. Matsagar, K. Seshagiri Rao, P. Sharma, and M Singh, "Character-ization of kota sandstone under different strain rates in uniaxial loading," *Geotechnical and Geological Engineering*, vol. 33, no. 1, pp. 1–10, 2015.

[9] Z. T. Bieniawaki, "Time-dependent behaviour of fractured rock," *Rock Mechanics and Rock Engineering*, vol. 2, no. 3, pp. 123–137, 1970.

[10] S. Peng and E. R. Podnieks, "Relaxation and the behavior of failed rock," *International Journal of Rock Mechanics and Mining Sciences & Geomechanics Abstracts*, vol. 9, no. 6, pp. 699-700, 1972.

[11] K. P. Chong, P. M. Hoyt, and J. W. Smith, "Effects of strain rate on oil shale fracturing," *International Journal of Rock Mechanics and Mining Sciences & Geomechanics Abstracts*, vol. 17, no. 1, pp. 35–43, 1980.

[12] S. Paulsen and Y. Nishimatsu, "Uniaxial compression testing using a linear combination of stress and strain as the control variable," *International Journal of Rock Mechanics and Mining Sciences & Geomechanics Abstracts*, vol. 22, no. 5, pp. 323–330, 1985.

[13] E. Z. Lajtai, E. J. S. Duncan, and B. J. Carter, "The effect of strain rate on rock strength," *Rock Mechanics and Rock Engineering*, vol. 24, no. 2, pp. 99–109, 1991.

[14] R. Vidya Sagar and M. V. M. S. Rao, "An experimental study on loading rate effect on acoustic emission based b-values related to reinforced concrete fracture," *Construction and Building Materials*, vol. 70, pp. 460–472, 2014.

[15] X.-p. Zhang, Q. Zhang, and S. Wu, "Acoustic emission characteristics of the rock-like material containing a single flaw under different compressive loading rates," *Computers and Geotechnics*, vol. 83, pp. 83–97, 2017.

[16] Y. Wang, S. Wu, and J. Zhou, "Experimental study on dynamic bending characteristics of dam concrete dynamic bending," *Nondestructive Testing*, vol. 31, no. 2, pp. 115–119, 2009.

[17] D. Jiang, J. Chen, S. Ren et al., "Experimental study on uniaxial strain rate effect and acoustic emission characteristics of salt rock," *Chinese Journal of Rock Mechanics and Engineering*, vol. 31, no. 2, pp. 326–336, 2012.

[18] G. Wang, G. Jing, C. Wang et al., "Study on rock rupture and acoustic emission response characteristics under different strain rates," *Coal Science and Technology*, vol. 155, no. 3, pp. 37–41, 2018.

[19] J. S. O. Lau and N. A. Chandler, "Innovative laboratory testing," *International Journal of Rock Mechanics and Mining Sciences*, vol. 41, no. 8, pp. 1427–1445, 2004.

[20] D. J. Holcomb and L. S. Costin, "Detecting damage surfaces in brittle materials using acoustic emissions," *Journal of Applied Mechanics*, vol. 53, no. 3, pp. 536–544, 1986.

[21] V. A. Mansurov, "Acoustic emission from failing rock behaviour," *Rock Mechanics and Rock Engineering*, vol. 27, no. 3, pp. 173–182, 1994.

[22] F. Wu, T. Liu, and J. Liu, "Excavation unloading destruction phenomena in rock dam foundations," *Bulletin of Engineering Geology and the Environment*, vol. 68, no. 2, pp. 257–262, 2009.

[23] K. Tang and M. Ohtsu, "Crack classification in concrete based on acoustic emission," *Construction and Building Materials*, vol. 24, no. 12, pp. 2339–2346, 2010.

[24] S.-H. Chang and C.-I. Lee, "Estimation of cracking and damage mechanisms in rock under triaxial compression by moment tensor analysis of acoustic emission," *International Journal of Rock Mechanics and Mining Sciences*, vol. 41, no. 7, pp. 1069–1086, 2004.

[25] A. Brzovic and E. Villaescusa, "Rock mass characterization and assessment of block-forming geological discontinuities during caving of primary copper ore at the El Teniente mine, Chile," *International Journal of Rock Mechanics and Mining Sciences*, vol. 44, no. 4, pp. 565–583, 2007.

[26] M. You and A. Hua, "Energy analysis of failure process of rock specimens," *Chinese Journal of Rock Mechanics and Engineering*, vol. 21, no. 6, pp. 778–781, 2002.

[27] C. Gao, X. Jin, P. He et al., "Study on mechanical properties of marble loading and unloading," *Chinese Journal of Rock Mechanics and Engineering*, vol. 24, no. 3, 2005.

[28] C. Wang, H. Zhou, S. He et al., "Study on the influence of unloading rate on the strength of beishan granite," *Rock and Soil Mechanics*, vol. 38, no. S2, pp. 151–157, 2017.

[29] Y. Cong, Z. Wang, Y. Zheng et al., "Study on acoustic emission characteristics of marble failure process under

unloading confining pressure path," *Journal of Southwest Jiaotong University*, vol. 49, no. 1, pp. 97–104, 2014.

[30] S. Qiu, X. Feng, C. Zhang et al., "Experimental study on unloading mechanical properties of deep buried marble under different unloading confining pressure rates," *Chinese Journal of Rock Mechanics and Engineering*, vol. 29, no. 9, pp. 1807–1817, 2010.

[31] M. Zhang, H. M. Lin, and L. D. WangZhou, "An experimental study of the damage characteristics of gas-containing coal under the conditions of different loading and unloading rates," *Journal of Loss Prevention in the Process Industries*, vol. 55, pp. 338–346, 2018.

[32] D. Wang, *Acoustic Emission Mutation and Prediction of Rock Triaxial Compression Fracture Instability*, Shandong University of Science and Technology, Qingdao, China, 2011.

[33] M. Huang, *Rock Damage Evolution Model and Damage Critical Value Theory and Experimental Research*, Central South University, Changsha, China, 2003.